

Use of Confocal Microscopy as a Nondestructive Method in the Study of Ink Jet Dot Formation

Tadeja Muck and Dejana Đorđević

Faculty of Natural Sciences and Engineering, Chair of Information and Graphic Technology, University of Ljubljana, SI-1000 Ljubljana, Slovenia
E-mail: tadeja.muck@ntf.uni-lj.si

Marko Kreft

Faculty of Medicine and Celica Biomedical Center, SI-1000 Ljubljana, Slovenia

Abstract. *The formation of the printing ink dot on the substrate is the final and the most critical phase in the printing process. The ink distribution on the printing surface and the drying mechanism depend on ink characteristics as well as on many other factors, for example, surface energy, roughness, sizing, and porosity. Suitable dot gain and high circularity (near unity) of printed dots predict the final print quality. High deviation from ideal circularity could cause undesired phenomena like wicking and bleeding. The aim of the present study is to determine ink dot formation by three different microscopic methods, optical microscopy (OM), scanning electron microscopy (SEM), and confocal laser scanning microscopy (CLSM). The main goal of the authors research was to evaluate the applicability of CLSM as a nondestructive method for three-dimensional visualization in the analysis of ink dot formation on UV ink jet prints. To validate the feasibility of such means in a three-dimensional context, the images obtained are compared to those obtained by traditional two-dimensional imaging systems such as OM and SEM. The authors show that the CLSM produces a replica of the cross-sectioned dot profile as seen in SEM. This means that the CLSM technique can be used to rapidly assess the dot profile without physical sectioning. © 2009 Society for Imaging Science and Technology.*

[DOI: 10.2352/J.ImagingSci.Technol.2009.53.4.040201]

INTRODUCTION

The basic concept of the confocal laser scanning microscopy (CLSM) was developed in the mid-1950s, but only in the late 1990s the concept was applied in broad number of applications.¹ CLSM uses pinholes to eliminate out of focus fluorescence, which results in an increase in contrast and resolution of the image. The stacks of optical sections taken at successive focal planes can be reconstructed to produce a three-dimensional (3D) view of a sample.² Applications of CLSM are already numerous in the life sciences^{2,3} and are increasing in materials sciences,^{4–6} including surface physics, papermaking, and printing sciences.

In the area of paper material sciences, applications include investigations in the field of physics of printing materials surface. With the use of CLSM, the macrosurface and microsurface structure has been investigated.^{4,7} Ozaki et al.⁸

used CLSM to characterize the depth of the coating layer penetration into the base paper; while in the field of papermaking, CLSM shows better evaluation than the conventional Parker print-surf method for the investigation of calendaring affects.⁴ Some published articles^{9,10} show the evaluation of roughness by CLSM as a function of the filler content in the sheet. Jang et al.¹¹ and Lepoutre and de Silveria¹² used CLSM to characterize coated layers.

A number of articles include applications in the field of printing science focused on the investigation of the ink transfer mechanism in conventional and digital printing technologies using 3D ink mapping made by CLSM.¹³ For prints made by electrophotography, CLSM provides a non-destructive method which could clearly show that when half-tone dots are deposited on the high areas of the paper surface, the toner adhesion is poor.

In the application of CLSM in ink jet printing, substantial work has been done to explain the ink-substrate interaction using nondestructive methods. A few studies have included the application of different spectroscopic and microscopic methods (Raman spectroscopy, Fourier transform infrared photoacoustic spectroscopy, and UV resonance Raman spectroscopy) in the study of ink distribution within the printed substrate.¹⁴

MATERIALS AND METHODES

Types of Printing Substrates

In the study, two different types of printing substrates were used as described in Table I. Printing was carried out with two different large format UV ink jet printers:

- (1) UV ink jet digital printer Durst Rho205 (resolution: 300 dpi, drop volume: 40 pL, CMYK inks, piezoink jet technology: print-on-demand) using Rho Ink Lightfast UV-curable pigment inks.
- (2) UV ink jet printing machine Grapo Octopus 1, with Xaar XJ500/40 printing head and Sunjet Crystal UFX™ inks. The printing characteristics were as follows: drop volume: 40 pL, resolution: 180 dpi (vertical), and 200 dpi (horizontal).

A printing test form with magenta color patches of 20%

Received Feb. 18, 2009; accepted for publication Apr. 10, 2009; published online Jun. 1, 2009.

1062-3701/2009/53(4)/040201/6/\$20.00.

Table I. Description of printing samples.

Sample mark	Sample description
Biomatt	Classical one side coated offset paper, grammage 150 g/m ²
Apco	Scheufelen's offset standard paper, coated, wood-free, and without fluorescent whitening agents, 150 g/m ²

and 100% raster tone values was prepared. A raster tone value is the percentage coverage by ink dots on the printing substrate. In the following text, the samples printed with Grapo Octopus 1 UV ink jet printer are denoted as G (Apco-G, Biomatt-G) and samples printed with Durst Rho205 UV ink jet printer are denoted as D (Biomatt-D).

Nondestructive Methods

CLSM

Printed samples were examined with a Zeiss confocal microscope (LSM 510, Jena, Germany). The measurements were done on printed samples soaked by immersion oil, which enabled the proper transparency of the samples, without destroying the sample.

Fluorescent images were acquired with a plano-apochromatic objective ($63\times f/1.4$ oil DIC) using the He/Ne laser with wavelength 533 nm and an argon laser with the wavelength 488 nm. Two excitation wavelengths were used to cover a broad spectrum of the dye fluorescence. Green and red emission lights were collected using the 505–530-nm-band-pass and 560-nm-long-pass filters, respectively. The z-axis resolution was 0.9 μm .

OM

The printed sample images were captured with a Leica EZ 4D optical microscope (OM) and charge coupled device camera at $35\times$ magnification. Two different sample exposures to light, and sidelight were used for eliminating light reflection from the magenta printed dots. Other imaging characteristics were captured format: 1600×1200 ppi; brightness: 90%; gamma: 0.80; saturation: 143.00; sharpening-on; and autowhite balance.

Destructive Method

SEM

The scanning electron microscope (SEM) JEOL JSM-6060LV was used with a magnification range from $95\times$ – $2000\times$. Strength of the electron beam was 10 kV. Since the substrate is nonconductive, the conventional method for coating samples with a conductive layer was used. Substrates for observation using the secondary electron detector were first carbon coated and then sputter coated with Au-Pd under high vacuum.

Cross-section Analysis with SEM

Cross-section analysis was used as a destructive method. The samples were immersed in liquid nitrogen and immediately broken in two by hand. Cross-section samples were also coated with conductive layer (described above) and captured by SEM.

Table II. Evaluation of the size of (average) printed dots in all three dimensions from optical cross-sections of captured samples.

Sample	X (μm)	Y (μm)	Z (μm)
Apco-G	105.9 ± 0.2	86.8 ± 0.1	17.3 ± 0.3
Biomatt-G	116.4 ± 0.1	112.2 ± 0.2	12.0 ± 0.2
Biomatt-D	145.8 ± 0.2	140.1 ± 0.3	21.3 ± 0.2

RESULTS AND DISCUSSION

The main focus of our research was the evaluation of printed dot formation with different microscopic methods. We evaluated the raster tone value (indirectly, dot gain) and also parameters focused on the formation of single raster dot: dot area, perimeter, and circularity. Physical dot gain arises from the excessive spread of the ink on the paper. For good print quality, dot gain has to be suitably low and the dot circularity should be near unity, where circularity = $4\pi(\text{dot area}/\text{perimeter}^2)$. Thus, 0 corresponds to low circularity and 1 corresponds to high circularity.

Nondestructive Methods

CLSM

All printed samples Apco-G, Biomatt-G, and Biomatt-D were examined with the Zeiss confocal microscope (LSM 510, Jena, Germany). For each sample, two captured images were analyzed. Three-dimensional pixel dimensions in all images were $x=0.4 \mu\text{m}$, $y=0.4 \mu\text{m}$, and $z=0.42 \mu\text{m}$.

The CLSM measurements of vertical ink distribution were done on the magenta printed area for each of the samples at 20% raster tone value. The computer software (LSM 510, Jena, Germany) displayed the vertical cross-section (z-direction) of the three-dimensional image. The maximum depth of penetrated ink was measured on cross-sections of all captured images from the top of the printed area (the most fluorescent part of the magenta dot) to the lowest visible ink trace in the sample. The evaluated average sizes of printed dots in all three dimensions from optical cross-sections of captured samples are given in Table II.

In all captured samples, the highest x-, y-, and z-dimensions of printed dots were evaluated. The x and y directions are parallel to the paper surface. For each measurement, three dots were analyzed. In the case of Apco-G and Biomatt-D samples, two different sizes of printed dots were observed (Figure 1). On the first evaluated sample (Apco-G), most of the dots and small stains were connected. In the sample Biomatt-D, the small stains and dots were separated. In our study, only the dots themselves were numerically evaluated (Table II). Table II also shows differences between samples printed with Durst UV ink jet printer (D) and samples printed with Grapo Octopus (G). Sample Biomatt-D produced on Durst printer has larger and thicker dots.

The images were captured with Zeiss LSM software and exported in TIFF format ready for image analyses using freely available software IMAGEJ (http://rsb.info.nih.gov/ink_jet/).

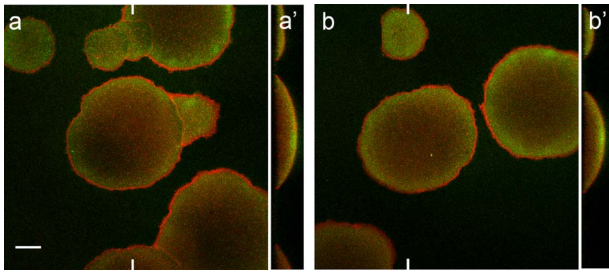


Figure 1. Printed dots on sample Apco-G. (a) Horizontal (x - y plane) optical cross-section of connected dots a': vertical (x - z plane) cross-section perpendicular to the section shown in (a); (b) and b' horizontal and vertical optical cross-sections of separated dots. Ticks on the edge of panels a and b are marking the positions of sections shown in a' and b'. Scale bar: 20 μm .

Table III. Evaluation of area, perimeter, and circularity for UV ink jet magenta printed dots with IMAGEJ.

Sample	Dot area (μm^2)	Perimeter (μm)	Circularity (-)
Apco-G	5466.4 ± 112.1	276.7 ± 50.1	0.90 ± 0.05
Biomatt-G	7403.1 ± 89.2	327.0 ± 32.3	0.88 ± 0.03
Biomatt-D	12105.4 ± 95.5	447.4 ± 25.2	0.76 ± 0.01

TIFF files were transformed into eight-bit images. All images were filtered with median filter (radius 2.0 pixels). A threshold was set via manual thresholding for each analyzed sample. The measuring scale was set in micrometers. The measured parameters were dot area, perimeter, and circularity of printed dots. The results of the image analysis are shown in Table III.

The results in Table III were based on three evaluated printed dots. They indicate that the dot area and perimeter of the printed dots are the highest on the sample Biomatt-D printed by Durst Rho printer (Figure 2). On the other hand, the dots on the same sample have the lowest circularity 0.76, in comparison with Biomatt-G, printed with Octopus UV ink jet printer, where dot circularity is much higher 0.88 (± 0.03).

OM

A representative captured sample, with 20% raster tone value and magnification 35 \times , is shown in Figure 3. To elimi-

nate the light reflection from the surface of printed dots, a sidelight for sample exposure was used. The captured image dimensions (x, y) were $3 \times 3 \text{ mm}^2$.

For print quality evaluation IMAGEJ software was used. Dot gain at the 20% raster tone value was evaluated. The dot gain, area, perimeter, and circularity of the average printed single raster dot were separately evaluated for each printed dot. For dot gain determination, the images were at first transformed into eight-bit images. Because of uneven exposure, images were then cropped to exclude the periphery of the image from the analysis. The starting picture area was 1600×1200 pixels and, after cropping, the dimensions were 800×800 pixels. For transformation into a binary image, "AUTO-THRESHOLD" was used and "Area Fraction" was calculated with IMAGEJ PLUGIN. For each evaluation six measurements were made. The results of dot gain determination at the 20% raster tone value are shown in Table IV. The highest dot gain is achieved on the sample Biomatt-G and the smallest on the sample Biomatt-D. These results show clear differences between inks of both printers.

The dot area, perimeter, and circularity of single raster dots were determined. First, the scale in μm was set. Then each single dot was separately evaluated by IMAGEJ macros. The results were given in Table V. From the results in Table V and in Figure 3, we can see that the formation of ink drop is the best on the Apco-G and the poorest on the Biomatt-D. A completely different order of precedence is achieved with the focus on the dot area or perimeter. The most desirable dot area and perimeter are achieved on the Biomatt-D and the smallest on the Apco-G. These results are in agreement with CLSM analysis (Table III).

Destructive Method

SEM

The printed samples captured by SEM were also evaluated by IMAGEJ software. At first, the raster tone value (the percentage of ink dots' coverage on the printing substrate) was determined. In Figure 4, SEM images for all three samples are shown. All SEM images were cropped to the final size of $800 \times 800 \mu\text{m}^2$. SEM images of all captured samples have the same ink/substrate contrast. This is the main reason why we decided to modify and upgrade our own macro for raster tone value evaluation (see Appendix). The results are presented in Table VI. The measurements were done on images

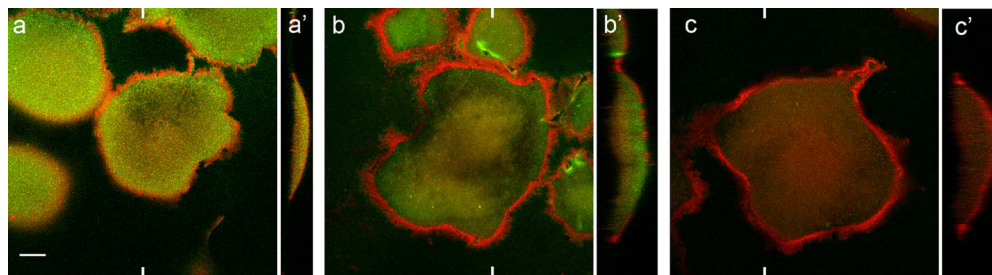
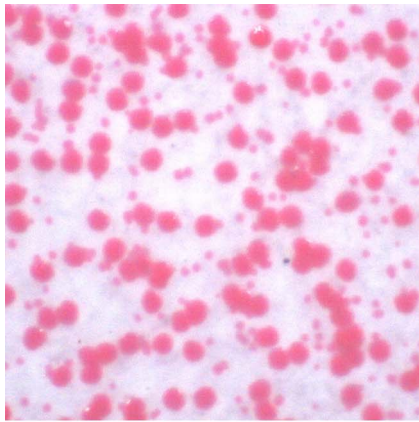
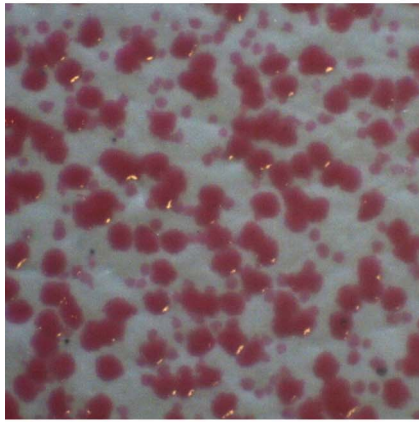


Figure 2. Printed dots on the sample Biomatt. Horizontal (x - y plane) optical cross-section of (a) Biomatt-G, (b) Biomatt-D with separated small stain and the dots, and (c) Biomatt-D with dot. a', b', and c': vertical (x - z planes) optical cross-sections perpendicular to the section shown in (a)-(c). Ticks on the edge of panels (a)-(c) are marking the positions of sections shown in a', b', and c'. Scale bar: 20 μm .



(a)



(b)



(c)

Figure 3. (a) Apco-G, (b) Biomatt-G, and (c) Biomatt-D printed with magenta UV ink at 20% raster tone value and captured by optical microscopy.

with 50 \times and 100 \times magnification. In this way, for each sample evaluation, two measurements were conducted. The results in Table VI are in agreement with the results from the evaluation of raster tone value and dot gain by the optical microscopy (Table IV).

Measurements of dot area, perimeter, and circularity were manually analyzed by using PLUGIN-ANALYZE particles. The results are shown in Table VII. Standard deviation is determined from five separate measurements. Finally, the

Table IV. Results of the raster tone value evaluation (percentage of ink dots' coverage) and dot gain (spreading of the ink) determined by OM.

Sample	Average A (%)	Dot gain ($\Delta A\%$)
Apco-G	30.10 \pm 0.30	10.10
Biomatt-G	42.79 \pm 0.57	22.79
Biomatt-D	26.61 \pm 0.41	6.61

Table V. Dot area, perimeter, and circularity of printed dots.

Sample	Dot area (μm^2)	Perimeter (μm)	Circularity (-)
Apco-G	5190.5 \pm 213.9	255.7 \pm 4.7	0.89 \pm 0.01
Biomatt-G	8007.9 \pm 189.3	328.9 \pm 10.4	0.73 \pm 0.10
Biomatt-D	13026.4 \pm 1901.7	442.8 \pm 38.2	0.64 \pm 0.09

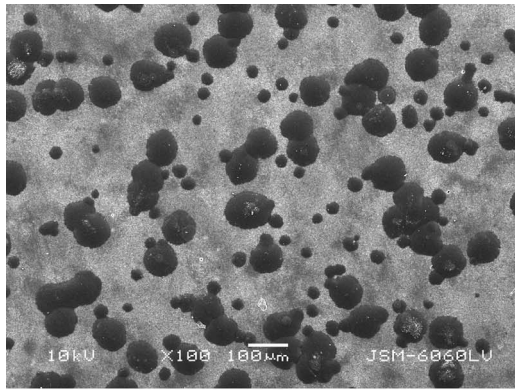
ink thickness (z -direction) was determined on two dots directly from the cross-sectioned samples by using the SEM image analysis tool. In Figures 5 and 6, measurements in the z -direction on samples Biomatt-G and Biomatt-D are shown.

On the sample Biomatt-G (Figure 5), the maximum ink thickness evaluated on the cross-sectioned sample is 11.8 μm , and on the sample Biomatt-D it is 20.4 μm . These measurements have shown high correlations with CLSM measurements of ink thickness in the z -dimension achieved by virtual cutting in the z -direction. With CLSM (Table I), the maximum ink thickness for sample Biomatt-G was (12.0 \pm 0.22) μm and for Biomatt-D (21.3 \pm 0.23) μm . This high correlation is achieved because of the suitable sample preparation.

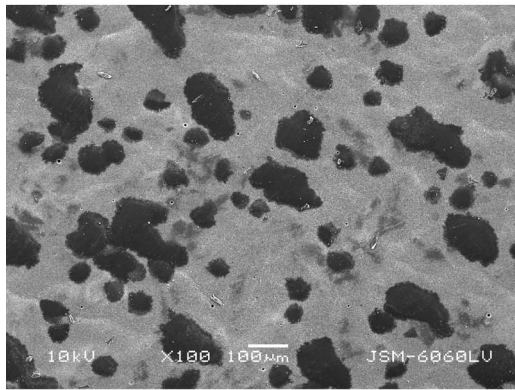
CONCLUSIONS

3D visualization of UV ink jet dots in a normal direction was achieved for samples soaked in immersion oil. In that way, reduced light scattering was achieved and a CLSM optical sectioning method could be used. In that manner, CLSM measurements of ink thickness layer have shown good agreement with the evaluation of ink penetration by destructive methods, e.g., cross-section analysis evaluated by SEM. Comparison of the results obtained from different microscopic methods for the determination of printed dot formation gives the same trend but different absolute values.

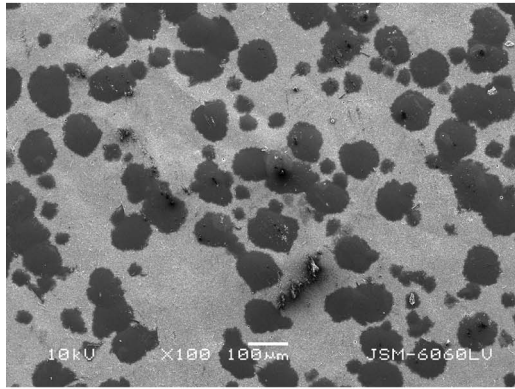
The differences in absolute values originate from different areas of analysis. For OM, 35 \times magnification was used; however, for SEM the magnification was 95 \times –2000 \times . CLSM evaluation was done on the area that is a little bit larger than one printed ink dot (206.83 \times 206.83 μm^2). The resolution in the z -direction is highly dependent on the numerical aperture of the objective used in CLSM, which in turn limits the field of view. It is too small for evaluating raster tone value and dot gain; on the other hand, the single



(a)



(b)



(c)

Figure 4. (a) APco-G, (b) Biomatt-G, and (c) Biomatt-D printed with magenta UV ink at 20% raster tone value and captured by SEM at 100X magnification.

Table VI. Results of the average raster tone values *A* (percent of ink's dots coverage) at 20% and dot gain (spreading of the ink) determined from SEM images.

Sample	Average <i>A</i> (%)	Dot gain (ΔA)
APco-G	34.88 ± 2.39	14.88
Biomatt-G	44.80 ± 0.39	22.80
Biomatt-D	29.51 ± 0.33	9.51

Table VII. Results of dot area, perimeter, and circularity for separated dots determined from SEM images.

Sample	Dot area (μm^2)	Perimeter (μm)	Circularity (-)
APco-G	5372.7 ± 492.4	303.0 ± 13.9	0.84 ± 0.08
Biomatt-G	7905.0 ± 390.9	365.1 ± 8.6	0.75 ± 0.05
Biomatt-D	14541.5 ± 2559.4	575.7 ± 117.2	0.62 ± 0.09

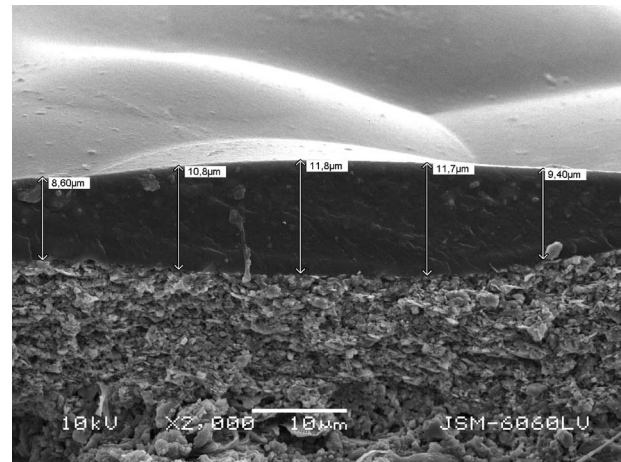


Figure 5. Cross-section of the sample Biomatt-G at 2000X magnification.

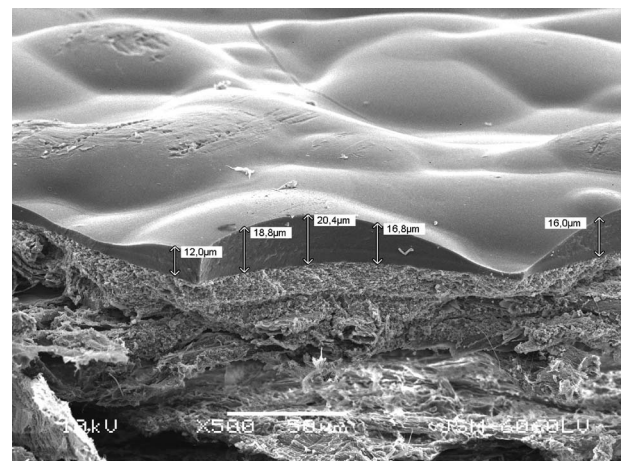


Figure 6. Cross-section of the sample Biomatt-D at 500X magnification.

dot formation and thickness could be determined by CLSM without destroying the sample.

OM is a nondestructive and quick method, which could give us information about raster tone value, dot gain, and also dot formation (single dot area, perimeter, and circularity); but the information in the *z*-direction could not be evaluated without cross-sectioning the samples. SEM is a destructive method, which also could give us good results for all parameters of interest; but it is a rather time consum-

ing method, insofar as we have to prepare a conductive coating layer on each evaluated sample.

The public domain IMAGEJ tools are very useful for the objective and automatic evaluation of images captured by different input microscopic devices (CLSM, OM, and SEM). Upgraded IMAGEJ MACRO for the calculation of the raster tone value can be used, after correct sampling and preparation procedures, as a relatively fast yet simple technique.

In conclusion, CLSM has great potential as a noncontacting and nondestructive tool. This means that the CLSM technique can be used to rapidly assess the dot profile. It may provide answers to many fundamental questions related to base and printed materials. Due to laser scanning of the entire surface, sampling is more complete compared to the traditional OM.

APPENDIX: MODIFIED MACRO FOR DOT AREA EVALUATION

```
run("Smooth");
run("Make Binary");
run("Median...", "radius=5");
run("Fill Holes");
if (bitDepth!=8)
    exit("This macro requires an 8-bit image");
white = 0;
black = 255;
getHistogram(0, hist, 256);
total = 0;
for (i=0; i<256; i++)
    total += hist[i];
print("");
print("Black pixels: " + hist[black]);
print("White pixels: " + hist[white]);
print("Percent black: " +100*hist[black]/total);
```

REFERENCES

- ¹N. S. Claxton, T. J. Fellers, and M. W. Davidson, Laser scanning confocal microscopy (<http://www.olympusconfocal.com/theory/LSCMIntro.pdf>).
- ²M. Krefť, M. Stenovec, M. Potokar, and R. Zorec, in *Image Analysis in Medical Microscopy and Pathology*, edited by H.-S. Wu and A. J. Einstein (Research Signpost, Kerala, 2007), pp. 193–206.
- ³S. Wilhelm, B. Grobler, M. Gluch, and H. Heinz, Confocal laser scanning microscopy principles (Microscopy from Carl Zeiss, microspspecial 40–617e/02.00, Jena).
- ⁴T. E. Conners and S. Banerjee, "Surface analysis of paper", in *Physical Characterization of Surfaces* (CRC Press, Boca Raton, FL, 1995), pp. 1–39.
- ⁵T. Muck, B. Lozo, L. Otahalova, M. Drůkova, and M. Kaplanova, "The use of non-destructive methods in the study of ink jet ink penetration", *Proc. TAGA* **4**, 1–11 (2007).
- ⁶A. Mauko, T. Muck, B. Mirtič, M. Krefť, and A. Mladenovič, in "Applicability of confocal laser scanning microscopy (CLSM) to geomaterials characterization with practical example of the determination of porosity in marble", in *11th Euroseminar on Microscopy Applied to Building Materials*, edited by I. Fernandes (Universidade do Porto, Porto, Portugal, 2007).
- ⁷A. E. Dixon, S. Damaskinos, A. Ribes, E. Seto, M. C. Bėland, T. Ueska, B. Darylmp, and S. P. M. Duttagupta, "Confocal scanning beam laser microscope: Applications requiring large data sets", *Proc. SPIE* **191**, 116–118 (1995).
- ⁸Y. Ozaki, D. W. Bousfield, and S. M. Shaler, "Three dimensional observation of coated paper by confocal laser scanning microscope", *Tappi J.* **5**(2), 3–8 (2006).
- ⁹W. W. Roehr, "Measurement and reduction of ink strike-through in newsprint", *Tappi J.* **49**, 255–259 (1966).
- ¹⁰R. R. Davidson, "Experiments on loading paper with low refractive index fillers", *Pap. Technol. (London)* **6**, 107–120 (1965).
- ¹¹H. F. Jang, A. G. Robertson, and R. S. Seth, "Optical sectioning of pulp fibers using confocal laser scanning microscopy", *Tappi J.* **74**, 217–219 (1991).
- ¹²P. Lepoutre and G. de Silveria, "Examination of cross-sections of blade and roll-coated LWC paper", *J. Pulp Pap. Sci.* **17**, J184–J186 (1991).
- ¹³Y. Bery, in *Advances in Printing Sciences and Technology*, edited by W. H. Banks (Pentech Press, London, 1982), Vol. **2**, pp. 206–234.
- ¹⁴B. Lozo, J. Vyřrykkā, T. Vuoirinen, and T. Muck, "Nondestructive microscopic and spectroscopic methods for depth profiling of ink jet prints", *J. Imaging Sci. Technol.* **50**, 333–340 (2006).